

Growth rate of the linear Richtmyer-Meshkov instability when a shock is reflected

J. G. Wouchuk

ETSI Industriales, Universidad de Castilla-La Mancha, 13071 Ciudad Real, Spain

(Received 27 December 2000; published 12 April 2001)

An analytic model is presented to calculate the growth rate of the linear Richtmyer-Meshkov instability in the shock-reflected case. The model allows us to calculate the asymptotic contact surface perturbation velocity for any value of the incident shock intensity, arbitrary fluids compressibilities, and for any density ratio at the interface. The growth rate comes out as the solution of a system of two coupled functional equations and is expressed formally as an infinite series. The distinguishing feature of the procedure shown here is the high speed of convergence of the intermediate calculations. There is excellent agreement with previous linear simulations and experiments done in shock tubes.

DOI: 10.1103/PhysRevE.63.056303

PACS number(s): 47.20.-k, 52.35.Py, 52.35.Tc

I. INTRODUCTION

The so-called Richtmyer-Meshkov (RM) instability [1,2] develops when a plane shock collides with a corrugated interface separating two different fluids. A shock is always transmitted and another shock or a rarefaction can be reflected back in the first fluid [3–5]. In this work, we concentrate only on the case in which a shock is reflected (see Refs. [3,4] to see which initial conditions should apply in order for a shock or a rarefaction to be reflected after the “incident shock-interface” interaction). Once the transmitted and reflected fronts have been formed and have started to separate from the contact surface at $t=0+$, the initial corrugation of the interface will begin to grow and the shock fronts will be deformed. As they move into the fluids, they leave density and vorticity perturbations behind them [4–7]. The interface velocity perturbations show damped oscillations, and when the fronts are far enough, the contact surface will reach a constant perturbed asymptotic velocity, which we call the asymptotic growth rate [3–5].

The precise determination of the asymptotic growth rate is a problem of fundamental importance in different fields of research, as in shock tube flows [7,8] and in inertial confinement fusion (ICF) [4–7]. Particularly in ICF, the growth of initial corrugations induced by the passage of shock waves is a major obstacle to the achievement of the proper conditions for fuel ignition at the end of the target implosion [5,9]. It is therefore easy to see the importance of understanding the physical mechanisms that drive or that could even stop the growth of this instability [3–7,9]. Quite recently, scientists working in this field have arrived at a general consensus as to the role that the vorticity generated by the shocks plays in the perturbation field evolution [5,7]. The linear theory predictions (essentially series expansions in terms of some adequate functions) agree with numerical simulations, despite the fact that former calculations overestimated the earlier experimental results in shock tubes [2,7,8]. Recently, a series of experiments with laser irradiation of solid foils has been performed [10]. In that way, the use of diaphragms to separate the fluids is avoided. The solids are quickly ionized and can be considered as ideal gases allowing the use of simple analytical models. The agreement of the experiments with the linear theory is satisfactory for the shots in which the

initial corrugation is sufficiently smaller than the corrugation wavelength. However, in these experiments a rarefaction instead of a shock wave is reflected back in the denser medium. It would be desirable for similar experiments for the shock-reflected case to be performed in the near future.

The analytical approaches to obtaining the asymptotic growth rate up to now have been of two different kinds. On the one side, we have rigorous linear theory in the form of series expansions, e.g., in terms of inverse powers of the Laplace variable “ s ” as in Fraley [11], in powers of time [4], or in terms of Bessel functions [6,12]. The inherent disadvantage in this method is that in order to obtain the growth rate with two or three significant digits, the series defining the velocity perturbation at the interface should contain many terms. Depending on the initial parameters of both fluids and on the incident shock intensity, the number could be larger than 50. Associated with the tedious task of solving hundreds of linear systems of equations, there is the problem of round-off error accumulation. To avoid it and obtain enough accuracy, we should start the calculations with high-precision arithmetics (above 70 digits [4]). The reason for such a huge number of coefficients is clear from the physics of the problem: these expansions are describing in detail all the sound-wave reverberations between the fronts and the interface. To keep track of the complete evolution far into the asymptotic stage, we need to follow all those reflections and refractions between the contact surface and the shocks. However, as we will see in the course of the work, in order to know the asymptotic perturbed velocity we can avoid such a fine description by using an iterative process that will demand many fewer calculations. The expansions discussed above could be truncated and only the first term could be retained in order to get a simple formula. However, the truncation is not trivial at all, and the price we pay is that the analytical formula so obtained will not be valid in the high compression limit. In fact, for stronger shocks or highly compressible fluids, or for a high-density contrast at the interface, the transmitted shock will take longer to separate from the interface than the reflected shock does [11,13]. This fact reinforces the importance of the sound-wave reflections addressed above. As the transmitted front “sees” the interface for a longer time, we cannot escape the need to describe that interaction, and therefore we cannot truncate the series

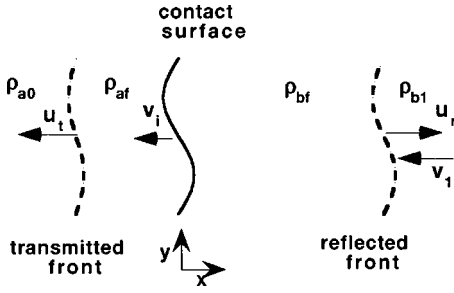


FIG. 1. Perturbed interface separating two different fluids after the interaction with an incident shock. For explanation of the symbols, see the text of the paper.

with just the first term. If we do so, we lose information that is relevant to the growth-rate calculation. Then we are in a trap: we cannot avoid calculating more and more terms as we approach the high compression limit, and this is because of the approach used, which needs an exact description of what happens at any time differential in order to reach the asymptotic stage. There is one possible way of getting out of the trap, which will be explained in the rest of the work.

As for the other kind of approach, it has been based on modifications of the known impulsive formula of Richtmyer [1,9]. In order to comment upon it, let us consider Fig. 1. An incident shock coming from the right inside fluid “b” hits the interface at $x=0$ and the transmitted and reflected fronts are formed at $t=0+$. The incident shock velocity is $-u_i\hat{x}$ (not shown) and has left fluid “b” moving with velocity $-v_i\hat{x}$. The interface acquires a velocity $-v_i\hat{x}$. The transmitted front moves with velocity $-u_t\hat{x}$ and the reflected shock speed is $+u_r\hat{x}$. These velocities are measured in the laboratory reference frame. We assume that the contact surface has an initial corrugation of the form $\psi_0 \cos ky$, before the shock-interface interaction. Here, $k=2\pi/\lambda$ is the perturbation wave number and λ is the perturbation wavelength. We assume that $\psi_0 \ll \lambda$ and therefore the linear theory is applicable.

According to the Richtmyer (R) prescription, the asymptotic growth rate δv_i^∞ can be calculated as

$$\delta v_i^\infty = \frac{\rho_{af} - \rho_{bf}}{\rho_{af} + \rho_{bf}} k \psi_{0f} v_i, \quad (1)$$

where ρ_{mf} is the shocked density of fluid “m” (“m” can be “a” or “b”) and $\psi_{0f} = \psi_0(u_i - v_i)/u_i$ is the shocked value of the interface corrugation at $t=0+$.

Quite recently, another heuristic approach has been proposed, also based on an impulsive model [9]. We call it the Vandenboomgaerde-Mügler-Gauthier (VMG) formula, and it can be written as

$$\delta v_i^\infty = \frac{1}{2} \left(\frac{\rho_{af} - \rho_{bf}}{\rho_{af} + \rho_{bf}} k \psi_{0f} + \frac{\rho_{a0} - \rho_{b0}}{\rho_{a0} + \rho_{b0}} k \psi_0 \right) v_i, \quad (2)$$

where ρ_{m0} is the preshock mass density of fluid “m.”

The degree of agreement of Eqs. (1) and (2) with the linear simulations and linear theory expansions has been studied in detail in former works [3–5,9]. The conclusion is

that the agreement is good for weak incident shocks and when the fluids are not very compressible at either side of the contact surface. However, there are exceptions in which either the R or the VMG prescriptions give a good estimate of the growth rate, but it is impossible to know it *a priori* [5]. Besides, there are situations in which the asymptotic growth equals zero and we say that the instability has been *frozen out* [3,5,14]. Unfortunately, the previous formulas do not predict correctly the freeze-out situations. As studied in Ref. [14], an accurate determination of freeze-out in the weak incident shock limit can be done on the basis of the analytical expression for the growth rate derived by Fraley [11]. However, the discussion is not valid at high compressions because his analytical formula is valid in the weak shock limit.

Summing up, the analytical methods discussed above pose different difficulties in the calculation of the growth rate for arbitrary values of the initial fluid parameters and incident shock strength. The traditional series expansions involve a large number of coupled linear equations with the corresponding problem of handling numerical rounding errors. Any analytical formula obtained from the truncation of those expansions will be strictly valid in the weak incident shock limit. The same thing happens with the heuristically derived formulas based on an impulsive description. Then, it is straightforward to recognize the importance of an analytical procedure that gives us the asymptotic growth rate without the mentioned problems.

In fact, as has been shown in Ref. [6] and discussed in Ref. [5], the growth rate can be exactly expressed in the following form:

$$\delta v_i^\infty = \frac{-\rho_{af} \delta v_{ya}^0 + \rho_{bf} \delta v_{yb}^0}{\rho_{af} + \rho_{bf}} + \frac{\rho_{af} F_a - \rho_{bf} F_b}{\rho_{af} + \rho_{bf}}, \quad (3)$$

where δv_{ym}^0 is the tangential velocity at the interface in fluid “m” just after shock-interface interaction at $t=0+$. The terms F_a and F_b represent the sonic interaction (important for $t>0+$) between the shock fronts and the contact surface. They can be written as integrals of the pressure perturbations along the shock front trajectories [5,6] or can also be seen as averaged measures of the vorticity field left by the corrugated fronts in the interior of the fluids [6]. Equation (3) is an exact result, valid in linear theory, and derived from first principles [5,6].

The first term on the right-hand side of Eq. (3) is due to the deposition of vorticity at the interface, at $t=0+$. It is the only important term in the limit of weak incident shocks, as will be shown later. It can be calculated immediately, without any knowledge of the instability evolution for $t>0+$. It is noted that it is obtained without any ad hoc assumption and without the need to resort to an impulsive formulation. Retaining only the first term in Eq. (3) is also equivalent to neglecting the vorticity generated by the shocks inside the fluids. It gives results similar to the impulsive prescriptions for very weak incident shocks.

The second term to the right in Eq. (3) comes into play for stronger shocks or highly compressible fluids, as well as when there is significant vorticity generation by the de-

formed fronts in the bulk of the fluids. It is also important in situations in which freeze-out occurs. It describes the interaction of the shock fronts with the corrugated interface. We see that they resume the information of the sound wave reverberations discussed before, and they do that in a quite economical way. Previous analytical formulas could not take into account the role played by the parameters F_a and F_b , and this fact could explain their partial failure at higher compressions. However, as discussed in Ref. [5], there was not an easy and straightforward method of calculating them until now. The only thing that could be done was to estimate them with the linear theory expansions addressed before. Sometimes only a small number of terms was enough, but this fact depended on the combination of initial parameters and the procedure was not at all easy to handle, precluding the direct use of Eq. (3). In this work, we show an exact analytical procedure with which to calculate the sonic interaction parameters F_a and F_b and hence to calculate the growth rate δv_i^∞ . The sonic parameters F_m come out as the solution of a system of two coupled functional equations. The details of solving this system in exact analytical terms are explained in full detail, so that the interested reader could apply the method to any other situation of interest. A distinguishing feature of the method developed here is the high speed of convergence of the iterations involved. The physical reasons for this will be explained during the work.

The present work is structured as follows. In Sec. II, we present the model. We subdivide it into two main subsections. In Sec. II A, only one fluid is considered with a corrugated shock moving to the right with a rippled interface at $x=0$. This case allows us to lay out the basic notation and to clearly describe the mathematical model to be used in the next subsection. Depending on the boundary conditions imposed at the left surface, we can study different related problems: the growth of perturbations for the case in which a shock hits a corrugated rigid wall [15] or even the symmetrical Riemann problem [5]. In Sec. II B, the model is applied to the more complicated situation in which a shock collides with the surface separating two fluids. The basic equations are obtained and the functional equations are solved. In Sec. III, we present comparisons with recent numerical simulations and experiments in shock tubes. A final discussion of the results and the physics underlying the model is given in Sec. IV.

II. CONSTRUCTION OF THE MODEL

In this section, we develop the model that allows us to calculate the growth rate of the RM instability. We divide it into two main subsections. In Sec. II A, the simpler problem of a single shock traveling in one fluid driven by a corrugated piston is addressed. This problem will help us to display the basic notation and prepare the building blocks upon which to construct the frame for the RM instability problem. In Sec. II B, the RM problem is fully discussed and an explicit analytical procedure for the growth rate evaluation is presented.

A. Shock driven by a corrugated piston

1. Boundary conditions at the shock and basic equations

We consider a shock wave moving to the right in fluid “ b ,” with speed U_r as measured in a frame at which the left piston surface is at rest. The shock front was at $x=0$ at $t=0+$. We do not specify the boundary conditions at the piston for the moment. Depending on the boundary conditions we choose there, we can study different situations of interest [16]. The fluid ahead of the shock is assumed to be homogeneous and moves with velocity $-v_0\hat{x}$ entering the shock. Its density ahead of the shock is ρ_{b1} and its value behind the shock is ρ_{bf} . The sound speed of the fluid between the piston and the shock is c_{bf} .

To study the perturbation field in the space delimited by the piston and the shock front, we use the following coordinate transformation, suggested by Briscoe and Kovitz [15]:

$$r_b \cosh \theta_b = kc_{bf}t, \quad (4)$$

$$r_b \sinh \theta_b = kx. \quad (5)$$

The piston surface has coordinate $\theta_i=0$ and the shock coordinate is defined by $\beta_r = \tanh \theta_r = U_r/c_{bf}$. It is not difficult to see that the pressure perturbations satisfy the linear wave equation in the space $0 \leq \theta_b \leq \theta_r$ [12,15]:

$$r_b \frac{\partial^2}{\partial r_b^2} \delta \hat{p}_b + \frac{\partial}{\partial r_b} \delta \hat{p}_b + r_b \delta \hat{p}_b = \frac{\partial}{\partial \theta_b} \left(\frac{1}{r_b} \frac{\partial}{\partial \theta_b} \delta \hat{p}_b \right), \quad (6)$$

where $\delta p_b = \rho_{bf} c_{bf} u_0 \delta \hat{p}_b$. The velocity u_0 is for the moment an arbitrary characteristic velocity of the unperturbed flow. It could be the sound speed of the shocked fluid “ b ” or the incident shock velocity. In Sec. III, we will use $u_0 = u_i$ (the incident shock speed) in order to compare with the results of Yang *et al.* [3].

We have found it convenient to define the following auxiliary function:

$$\delta h_b = \frac{1}{r_b} \frac{\partial}{\partial \theta_b} \delta \hat{p}_b. \quad (7)$$

For any quantity $\delta \phi_b(\theta_b, r_b)$, we define its Laplace transform by

$$\delta \Phi_b(\theta_b, s_b) = \int_0^\infty \exp(-s_b r_b) \delta \phi_b(\theta_b, r_b) dr_b. \quad (8)$$

According to Eq. (8) and changing to the variable $s_b = \sinh q_b$, the former Eqs. (6) and (7) can be rewritten as

$$\frac{\partial}{\partial q_b} (\cosh q_b \delta P_b) + \frac{\partial}{\partial \theta_b} \delta H_b = 0, \quad (9)$$

$$\frac{\partial}{\partial q_b} \delta H_b + \frac{\partial}{\partial \theta_b} (\cosh q_b \delta P_b) = 0. \quad (10)$$

Changing to the variables $q_b + \theta_b$ and $q_b - \theta_b$, we can easily find a first integral of the above system of differential equations:

$$\begin{aligned} \delta H_b(\theta_b, q_b + \theta_b) + \cosh(q_b + \theta_b) \delta P_b(\theta_b, q_b + \theta_b) \\ = F_{b1}(q_b), \end{aligned} \quad (11)$$

$$\begin{aligned} -\delta H_b(\theta_b, q_b - \theta_b) + \cosh(q_b - \theta_b) \delta P_b(\theta_b, q_b - \theta_b) \\ = F_{b2}(q_b), \end{aligned} \quad (12)$$

for some unknown functions F_{b1} and F_{b2} . We see that the left-hand sides of the preceding equations do not depend on the coordinate θ_b . Thus, we can write

$$F_{b1}(q_b) = \delta H_{bi}(q_b) + \cosh q_b \delta P_{bi}(q_b), \quad (13)$$

$$F_{b2}(q_b) = -\delta H_{bi}(q_b) + \cosh q_b \delta P_{bi}(q_b), \quad (14)$$

where $\delta P_{bi}(q_b) = \delta P_b(\theta_b = 0, q_b)$ and $\delta H_{bi}(q_b) = \delta H_b(\theta_b = 0, q_b)$ are the pressure perturbations at the left piston surface.

We can write Eqs. (11)–(14) as

$$\begin{aligned} \delta H_b(\theta_b, q_b + \theta_b) + \cosh(q_b + \theta_b) \delta P_b(\theta_b, q_b + \theta_b) \\ = \delta H_{bi}(q_b) + \cosh q_b \delta P_{bi}(q_b), \end{aligned} \quad (15)$$

$$\begin{aligned} -\delta H_b(\theta_b, q_b - \theta_b) + \cosh(q_b - \theta_b) \delta P_b(\theta_b, q_b - \theta_b) \\ = -\delta H_{bi}(q_b) + \cosh q_b \delta P_{bi}(q_b). \end{aligned} \quad (16)$$

It is at this point that we can distinguish different cases. As far as the coordinate θ_b is concerned, it is arbitrary in the preceding two equations. We have to write boundary conditions at the shock front and at the piston surface. From the linearized Rankine-Hugoniot conditions at the shock front, we can relate δH_b with δP_b . This will be done in the next paragraph. By imposing appropriate functions for δH_{bi} and δP_{bi} , we can model different situations [5,16].

2. Boundary conditions at the shock front

It can be seen after some tedious algebra that the linearized Rankine-Hugoniot conditions can be put in the form [1,6,12]

$$\delta H_b(\theta_r, q_b) = \alpha_{b1}(q_b) \delta P_b(\theta_r, q_b) + \alpha_{b2}(q_b), \quad (17)$$

where

$$\alpha_{b1}(q_b) = -\chi_b \sinh q_b - \frac{1}{2} \frac{\beta_r}{\kappa_r} \frac{\kappa_r - \beta_r^2}{1 - \beta_r^2} \frac{\rho_{bf}}{\rho_{b1}} \frac{1}{\sinh q_b}, \quad (18)$$

$$\alpha_{b2}(q_b) = -\delta v_{yb}^0 \frac{\sinh \theta_r}{\sinh q_b}, \quad (19)$$

with

$$\chi_b = \frac{\kappa_r + \beta_r^2}{2\kappa_r\beta_r}, \quad (20)$$

and

$$\kappa_r = \frac{1}{c_{bf}^2} \left(\frac{dp}{d\rho} \right)_{\rho_{bf}}. \quad (21)$$

The derivative in Eq. (21) is evaluated along the Hugoniot curve at the final state of fluid ‘‘b.’’ For an ideal gas with isentropic exponent γ_b , it is

$$\frac{1}{\kappa_r} = \frac{1}{4} (\gamma_b - 1)^2 (1 + z_r) \frac{\rho_{bf}}{\rho_{b1}} \left[1 - \frac{\rho_{b1}}{\rho_{bf}} \left(\frac{\gamma_b + 1}{\gamma_b - 1} \right) \right]^2, \quad (22)$$

where $z_r = (p_2 - p_1)/p_1$ is the shock intensity of the reflected front. The pressure p_2 is the pressure behind it, and p_1 is the pressure ahead of it.

Before closing this subsection, it will be useful for future discussion to note that the value of $\delta P_b(\theta_r, q_b = 0)$ can be calculated exactly. In fact, if we take the limit $q_b \rightarrow 0$ in Eqs. (17)–(19), we get the following result:

$$\begin{aligned} \delta P_b(\theta_r, q_b = 0) &= -\lim_{q_b \rightarrow 0} \frac{\alpha_{b2}(q_b)}{\alpha_{b1}(q_b)} \\ &= 2 \delta v_{yb}^0 \sinh \theta_r \frac{\kappa_r}{\beta_r} \frac{1 - \beta_r^2}{\kappa_r - \beta_r^2} \frac{\rho_{b1}}{\rho_{bf}}. \end{aligned} \quad (23)$$

3. Asymptotic properties of the velocity perturbation field

We write the velocity perturbations in the form $\delta v_x = u_0 \delta u \cos ky$ for the normal velocity perturbations and $\delta v_y = u_0 \delta v \sin ky$ for the tangential velocity perturbations. Besides, the vorticity generated by the shocks at the position (x, y) can be written as [6,12]

$$\delta \omega_b(x, y) = k u_0 g_b(kx) \sin ky, \quad (24)$$

where the function g_b is given by

$$g_b(kx) = \Omega_b \delta \hat{p}_b \left(\theta_r, r_b = \frac{kx}{\sinh \theta_r} \right), \quad (25)$$

with

$$\Omega_b = -\frac{1}{2\beta_r} \left(1 - \frac{\beta_r^2}{\kappa_r} \right) \frac{v_0}{U_r}. \quad (26)$$

That is, the vorticity at the position (x, y) is the vorticity generated by the rippled shock front at the instant of time $t_0(x) = x/U_r$ when it arrived at that point.

It is not difficult to see that δu and δv satisfy the inhomogeneous wave equations:

$$\frac{\partial^2}{\partial (kc_{bf}t)^2} \delta u - \frac{\partial^2}{\partial (kx)^2} \delta u + \delta u = g_b(kx), \quad (27)$$

$$\frac{\partial^2}{\partial(kc_{bf}t)^2} \delta v - \frac{\partial^2}{\partial(kx)^2} \delta v + \delta v = - \frac{\partial}{\partial kx} g_b(kx). \quad (28)$$

In the asymptotic limit ($t \rightarrow \infty$) when the partial time derivatives vanish, the last two equations can be written

$$\frac{d^2}{d(kx)^2} \delta u - \delta u = -g_b(kx), \quad (29)$$

$$\frac{d^2}{d(kx)^2} \delta v - \delta v = \frac{d}{dkx} g_b(kx). \quad (30)$$

Let us concentrate on Eq. (29). If we multiply both members by $\exp(-\sigma kx)$ and integrate between $0 \leq kx < \infty$, we are Laplace-transforming that equation and we obtain

$$\begin{aligned} (\sigma^2 - 1) \delta U - \sigma \delta u(x=0) - \delta u'(x=0) \\ = -\Omega_b \sinh \theta_r \delta P_b(\theta_r, s_b = \sigma \sinh \theta_r). \end{aligned} \quad (31)$$

For simplicity, from now on we will write $\delta P_b(\theta_r, s_b) = \delta P_r(s_b)$. The quantity $\delta u(x=0)$ is the asymptotic normal velocity at the piston surface and we call it δv_i^∞ . The quantity $\delta u'(x=0)$ is equal to minus the asymptotic tangential velocity at the piston: $-\delta v_{yb}^\infty$ (because of the asymptotic incompressibility of the perturbation velocity field).

If we do a similar manipulation in Eq. (30), we can recast the preceding two equations in the form

$$\delta U(\sigma) = \frac{\sigma \delta v_i^\infty - \delta v_{yb}^\infty - \Omega_b \sinh \theta_r \delta P_r(s_b = \sigma \sinh \theta_r)}{\sigma^2 - 1}, \quad (32)$$

$$\delta V(\sigma) = \frac{\sigma \delta v_{yb}^\infty - \delta v_i^\infty + \Omega_b \sigma \sinh \theta_r \delta P_r(s_b = \sigma \sinh \theta_r) - \Omega_b \sinh \theta_r \hat{\delta p}_r(0+)}{\sigma^2 - 1}, \quad (33)$$

where $\hat{\delta p}_r(0+)$ is the value of the shock pressure perturbation at $t=0+$. In the cases of interest in this work, its value is 0 [1,3,4,6].

Once the shock has traveled a distance that is large compared with the corrugation wavelength, the pressure perturbations will become negligible. We therefore require vanishing of the velocity perturbations at $x \rightarrow \infty$. We thus deduce from either of the preceding two equations

$$\delta v_i^\infty - \delta v_{yb}^\infty = \Omega_b \sinh \theta_r \delta P_r(s_b = \sinh \theta_r). \quad (34)$$

We see that the tangential and normal velocities at the left boundary are not independent, but are related through the time history of the pressure perturbations at the shock front since $t=0+$ up to $t=\infty$. That is, their difference is a function of the compressibility of the fluid and of the shock strength. If we want to know about any one of them, we must get the value of δP_r and evaluate it at $q_b = \theta_r$.

We study two different cases, one in which the normal velocity is zero at the piston surface at all times (a rigid wall) and another case in which we cause the pressure perturbations to vanish at the piston (symmetrical Riemann problem).

4. Shock reflection from a corrugated rigid wall

If we impose $\delta H_{bi} = 0$, we can model the reflection of an incident shock from a sinusoidally corrugated rigid wall at $x=0$ [15].

After some algebra, we get

$$\delta P_r(q_b) = \lambda_{b1}(q_b) + \lambda_{b2}(q_b) \delta P_r(q_b + 2\theta_r), \quad (35)$$

with

$$\lambda_{b1}(q_b) = \frac{\alpha_{b2}(q_b) + \alpha_{b2}(q_b + 2\theta_r)}{\cosh q_b - \alpha_{b1}(q_b)}, \quad (36)$$

$$\lambda_{b2}(q_b) = \frac{\alpha_{b1}(q_b + 2\theta_r) + \cosh(q_b + 2\theta_r)}{\cosh q_b - \alpha_{b1}(q_b)}. \quad (37)$$

The functional equation displayed in Eq. (35) can be rewritten in operator form as [17,18]

$$\delta P_r(q_b) = \lambda_{b1}(q_b) + \lambda_{b2}(q_b) e^{2\theta_r D_b} \delta P_r(q_b), \quad (38)$$

where $D_b = d/dq_b$. The exponential factor in the preceding equation should be understood as a translation operator acting on the function to its right, shifting its argument in the amount $2\theta_r$ [17,18].

A formal solution is obtained at once,

$$\delta P_r(q_b) = [1 - \lambda_{b2}(q_b) e^{2\theta_r D_b}]^{-1} \lambda_{b1}(q_b). \quad (39)$$

After a Taylor expansion, we get

$$\delta P_r = \lambda_{b1}(q_b) + \sum_{j=1}^{\infty} \lambda_{b1}(q_b + 2j\theta_r) \prod_{l=0}^{j-1} \lambda_{b2}(q_b + 2l\theta_r). \quad (40)$$

It is easy to prove that the above function satisfies the preceding functional equation. Evaluating δP_r at $q_b = \theta_r$, we get the asymptotic tangential velocity at the piston surface using Eq. (34), because the normal velocity is zero there. However, before doing that, we note that a faster evaluation of δP_r can be done solving Eq. (35) by iteration with a good choice for the starting function.

We consider Eq. (35) in the limit $q_b \gg \theta_r$. We get in this way an approximate solution, which we call $\delta P_r^{[0]}$. This ap-

proximate function is obtained by neglecting $2\theta_r$ compared to q_b inside the argument of δP_r in Eq. (35). However, we do not neglect it inside the arguments of the functions $\lambda_{b1,2}$ as this improves the overall convergence. The approximate function with which we start the iteration is

$$\delta P_r^{[0]} = \frac{\lambda_{b1}(q_b)}{1 - \lambda_{b2}(q_b)}. \quad (41)$$

We can easily check that this function has the correct value at $q_b=0$. In fact, we take the limit $q_b \rightarrow 0$ in the above function and verify that $\delta P_r^{[0]}(q_b=0) = \delta P_r(q_b=0)$ as given in Eq. (23).

Once we have the initial trial function, we build the iteration sequence:

$$\delta P_r^{[n]}(q_b) = \lambda_{b1}(q_b) + \lambda_{b2}(q_b) \delta P_r^{[n-1]}(q_b + 2\theta_r). \quad (42)$$

Therefore, we can write

$$\begin{aligned} \delta P_r = & \lambda_{b1} + \lim_{n \rightarrow \infty} \left(\sum_{j=1}^n \left[\lambda_{b1}(q_b + 2j\theta_r) \prod_{l=0}^{j-1} \lambda_{b2}(q_b + 2l\theta_r) \right] \right. \\ & \left. + \prod_{l=0}^n \lambda_{b2}(q_b + 2l\theta_r) \delta P_r^{[0]}(q_b + 2n\theta_r) \right). \end{aligned} \quad (43)$$

Equation (43) is a solution of the functional equation, because the last term tends to zero for any value of q_b in the limit $n \rightarrow \infty$.

The advantage of using the sequence of iterated functions $\delta P_r^{[0]}, \dots, \delta P_r^{[n]}, \dots$ is the high speed of convergence that can be obtained. There are physical reasons for this. In fact, as we have shown before and because of the way in which we constructed the starting function, $\delta P_r^{[0]}$ satisfies the functional equation in the limit $q_b \gg \theta_r$ and also has the correct value at $q_b=0$. But, these limits correspond to the limits $s_b = \infty$ and $s_b = 0$ in the Laplace variable. We know from the theory of the Laplace transformation that these limits are equivalent to the limits $t \rightarrow 0+$ and $t \rightarrow \infty$. Let us say it in other words: the starting function we are using conveys exact physical information of the shock front pressure perturbations both at early and large times. The iteration process actually smoothes the difference between the successive iteration functions and the true solution to the functional equation in such a way as to properly satisfy the boundary conditions at the shock and at the piston surface. Taking these facts into account, it is natural to foresee that the iteration process should be quite fast. To accelerate convergence, the nature of the functional equation itself is helpful. Indeed, the essence of solving the functional equation is to evaluate the iterated sequence of approximate functions at successively shifted values of their arguments (terms like $2j\theta_r$, for instance). If we pay attention to the fact that the initial trial function and the chain of iterated functions behave as decaying exponentials at large values of their arguments, we see that the corresponding correction terms will be smaller and smaller as we go deeper in the iteration chain. This peculiarity will be confirmed later on when we discuss the results,

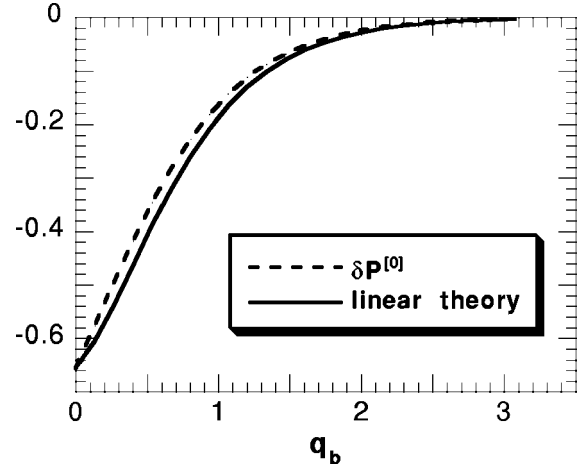


FIG. 2. Laplace transform of the shock front pressure perturbations for reflection at a rigid wall. For details, see the text of the paper.

either for the single shock moving into only one fluid or for the more complicated case of two shocks moving in different fluids (the RM instability problem).

In Fig. 2, we show the results for a plane shock that has been reflected at a sinusoidally rippled wall. The gas is air ($\gamma_{\text{air}}=1.4$) and the incident shock Mach number is 10. The dotted line is the starting function $\delta P_r^{[0]}$ and the solid line is the linear theory prediction, which agrees with the second iterated function $\delta P_r^{[2]}$. The normalizing speed here is $u_0 = u_i$. For the tangential velocity at the piston, we get $\delta v_{yb}^\infty = 0.4519k\psi_0 u_i$, calculated either from Eq. (34) (using $n=2$ in the iteration sequence) or from the linear theory expansions [12].

5. Perturbed symmetrical Riemann problem

Let us consider now a different boundary condition at the left surface. We require $\delta P_{bi}=0$, that is, the vanishing of the pressure perturbations themselves rather than the pressure gradient at $x=0$. It is clear that the normal velocity will reach a final asymptotic value in this case. However, the piston tangential velocity perturbation will always stay at its initial value $\delta v_{yb}^\infty = \delta v_{yb}^0$. This idealized situation could correspond, as discussed in Ref. [5], to the collision of two identical foils with an initial corrugation at the surface of contact and represents another case of the perturbed symmetrical Riemann problem in gas dynamics [5]. The only mathematical difference in this case is the difference in the boundary condition on the piston surface. After some algebra, it can be seen that the functions $\lambda_{b1,2}$ should be changed by

$$\lambda_{b1}(q_b) = \frac{-\alpha_{b2}(q_b) + \alpha_{b2}(q_b + 2\theta_r)}{\cosh q_b - \alpha_{b1}(q_b)}, \quad (44)$$

$$\lambda_{b2}(q_b) = -\frac{\alpha_{b1}(q_b + 2\theta_r) + \cosh(q_b + 2\theta_r)}{\cosh q_b - \alpha_{b1}(q_b)}. \quad (45)$$

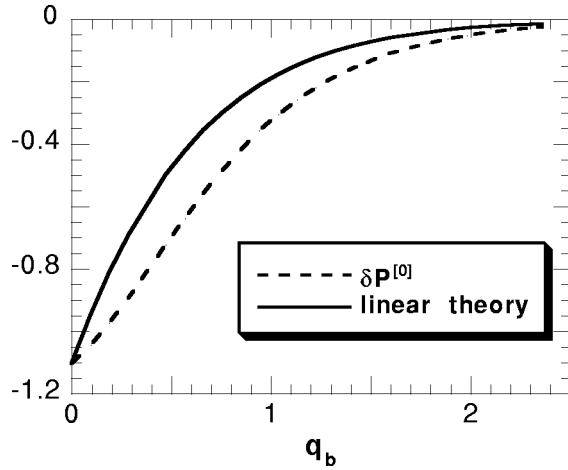


FIG. 3. Laplace transform of the shock front pressure perturbations for the perturbed symmetrical Riemann problem. For details, see the text of the paper.

The procedure to construct the functional equation and the iteration sequence of approximate solutions is the same as discussed before. We do not repeat those calculations again. Instead, in Fig. 3 we consider a shock moving into a gas with $\gamma_b = 1.1$ and the fluid entering the shock moves with a velocity $v_0 = -10c_{b1}\hat{x}$, where c_{b1} is the sound speed of the fluid in front of the shock. We show the approximate function $\delta P_r^{[0]}$ with dotted lines. The solid line corresponds to the linear theory prediction, which coincides with the iterated function $\delta P_r^{[4]}$. The asymptotic growth rate derived from Eq. (34) (with $n=4$ in the iteration sequence) is $\delta v_i^\infty = 0.452k\psi_0v_0$, which agrees with the linear theory prediction.

Another boundary condition could be imposed on the piston surface at $x=0$. For example, we could have an exponentially time-varying pressure perturbation, as discussed in Velikovich *et al.* [16]. Also, we could consider the leakage of mass at the left piston to model a rippled shock driven by ablation [16,19,20]. However, this task exceeds the scope of the present paper and will not be considered here.

B. Richtmyer-Meshkov (RM) instability problem

1. Formulation of the functional equations

We refer the reader again to Fig. 1. To get the growth rate at $x=0$, we have at our disposal Eq. (34) and its partner equation in fluid ‘‘a’’

$$-\delta v_i^\infty + \delta v_{yb}^\infty = F_b = \Omega_b \sinh \theta_r \delta P_r(q_b = \theta_r), \quad (46)$$

$$\delta v_i^\infty + \delta v_{ya}^\infty = F_a = -\Omega_a \sinh \theta_t \delta P_t(q_a = -\theta_t), \quad (47)$$

where $\beta_t = -\tanh \theta_t = (u_t - v_t)/c_{af}$ and c_{af} is the final sound speed of fluid ‘‘a.’’ (Remember that the transmitted shock coordinate θ_t is negative because the positive \hat{x} direction points inside fluid ‘‘b.’’) Besides,

$$\Omega_a = -\frac{1}{2\beta_t} \left(1 - \frac{\beta_t^2}{\kappa_t} \right) \frac{v_i}{u_t - v_i} \quad (48)$$

and

$$\kappa_t = \frac{1}{c_{af}^2} \left(\frac{dp}{d\rho} \right)_{\rho_{af}}, \quad (49)$$

and the last derivative is taken along the Hugoniot adiabat. The expression of the parameter κ_t for an ideal gas with isentropic exponent γ_a is

$$\frac{1}{\kappa_t} = \frac{1}{4} (\gamma_a - 1)^2 (1 + z_t) \frac{\rho_{af}}{\rho_{a0}} \left[1 - \frac{\rho_{a0}}{\rho_{af}} \left(\frac{\gamma_a + 1}{\gamma_a - 1} \right) \right]^2. \quad (50)$$

The quantity $z_t = (p_2 - p_0)/p_0$ is the transmitted shock intensity, with p_2 the pressure behind the transmitted front and p_0 the pressure ahead of it.

It is adequate to briefly discuss here the limit of very weak incident shocks. It can be seen after some straightforward algebra that in the weak shock limit, the quantities Ω_a and Ω_b are of second order in the corresponding shock intensities (z_t and z_r , respectively). This explains why the bulk vorticity is not significant for the growth rate calculation in this limit. Let us consider the parameter F_a : the quantity $\sinh \theta_t$ scales like $1/z_t^{1/2}$ for very small values of z_t . The quantity Ω_a scales like z_t^2 , as can easily be seen from Eq. (48), and the quantity $\delta P_t(q_a = -\theta_t)$ scales like $z_t^{3/2}$, always for very weak incident shocks. It is clear that by taking all these scalings into account in the definition of F_a [Eq. (47)], we get a dependence of the form $F_a \sim z_t^3$. Similar reasonings hold for the symmetrical parameter F_b on the other side of the contact surface: $F_b \sim z_r^3$. Therefore, for very weak incident shocks, the sonic parameters can be safely neglected when compared to the initial shear velocities at the interface (δv_{ya}^0 and δv_{yb}^0), as these tangential velocities are of first order in the shock intensity. Obviously, these considerations do not apply for shocks of finite intensity and the sonic parameters could not be neglected in the general case.

We can take Eqs. (46) and (47) as the formal definitions of the sonic parameters F_m . We thus see that the normal and tangential velocities at both sides of the interface are related to each other through the compressible evolution of the shock front pressure perturbations in the whole time interval $0 + \leq t < \infty$. And here we should note that thanks to the specific form of the parameters F_m , we are able to conserve thought and effort. Actually, the sonic parameters as defined above are just integrals of the time-oscillating shock front pressure perturbations. Due to this simple fact, we will dispense with describing the exact details of these oscillations in the real physical space. The price we pay for that simplification is that we must work within the parameters of the abstract quantities q_a and q_b , thus losing, perhaps, some intuition in the process. However, it is important to realize that in order to arrive at the asymptotic growth rate, we actually need less detailed information than the former studies using series expansions might have indicated. Of course, that information still exists inside the integrals (we are not delet-

ing it from the problem) but we will find the way to do those integrals without the explicit calculation of the real shock pressure perturbations in the time domain. We just need to take a smooth average of these pressure perturbations in the space defined by the variables q_a and q_b . The associated functions (δP_r and δP_t) in these abstract spaces do not oscillate. At most, they decay exponentially at large values of the corresponding variables. As we will see later on, these facts together with a good choice of the iteration scheme will lead us to a quite fast calculation technique.

Before solving for the functions δP_r and δP_t , we note that we need an additional equation, since we still have three unknown velocities (namely, δv_i^∞ , δv_{ya}^∞ , and δv_{yb}^∞). This additional equation comes from the integration in time of the tangential momentum conservation at the contact surface, requiring pressure continuity during the whole instability evolution [6,12],

$$\int_{0+}^{\infty} \rho_{af} \frac{\partial}{\partial t} \delta v_{ya} dt = \int_{0+}^{\infty} \rho_{bf} \frac{\partial}{\partial t} \delta v_{yb} dt. \quad (51)$$

We get

$$\rho_{af}(\delta v_{ya}^\infty - \delta v_{ya}^0) = \rho_{bf}(\delta v_{yb}^\infty - \delta v_{yb}^0). \quad (52)$$

Combining Eqs. (46), (47), and (52), we finally arrive at Eq. (3),

$$\delta v_i^\infty = \frac{-\rho_{af} \delta v_{ya}^0 + \rho_{bf} \delta v_{yb}^0}{\rho_{af} + \rho_{bf}} + \frac{\rho_{af} F_a - \rho_{bf} F_b}{\rho_{af} + \rho_{bf}}.$$

We still need the quantities $\delta P_r(q_b = \theta_r)$ and $\delta P_t(q_a = -\theta_t)$. The next task will be to formulate the corresponding coupled functional equations for the pressure perturbations $\delta P_r(q_b)$ and $\delta P_t(q_a)$.

For fluid ‘‘a,’’ the same reasonings as in the preceding subsection apply. That is, we will arrive at a system of equations similar to Eqs. (11) and (12):

$$\begin{aligned} \delta H_a(\theta_a, q_a + \theta_a) + \cosh(q_a + \theta_a) \delta P_a(\theta_a, q_a + \theta_a) \\ = F_{a1}(q_a), \end{aligned} \quad (53)$$

$$\begin{aligned} -\delta H_a(\theta_a, q_a - \theta_a) + \cosh(q_a - \theta_a) \delta P_a(\theta_a, q_a - \theta_a) \\ = F_{a2}(q_a), \end{aligned} \quad (54)$$

where the functions F_{a1} and F_{a2} have to be determined.

As the right-hand sides of the preceding equations are independent of θ_a , we can evaluate the preceding equations at $\theta_a = 0$ (the contact surface) and write a system similar to Eqs. (15) and (16):

$$\begin{aligned} \delta H_a(\theta_a, q_a + \theta_a) + \cosh(q_a + \theta_a) \delta P_a(\theta_a, q_a + \theta_a) \\ = \delta H_{ai}(q_a) + \cosh q_a \delta P_{ai}(q_a), \end{aligned} \quad (55)$$

$$\begin{aligned} -\delta H_a(\theta_a, q_a - \theta_a) + \cosh(q_a - \theta_a) \delta P_a(\theta_a, q_a - \theta_a) \\ = -\delta H_{ai}(q_a) + \cosh q_a \delta P_{ai}(q_a), \end{aligned} \quad (56)$$

where $\delta H_{ai} = \delta H_a(\theta_a = 0)$ and $\delta P_{ai} = \delta P_a(\theta_a = 0)$. Furthermore, the continuity of pressure and normal acceleration at the contact surface are written as

$$\delta H_{ai}(q_a) = \delta H_{bi}(q_b), \quad (57)$$

$$\rho_{af} \delta P_{ai}(q_a) = \rho_{bf} \delta P_{bi}(q_b), \quad (58)$$

where $c_{af} \sinh q_a = c_{bf} \sinh q_b$. Besides, the linearized Rankine-Hugoniot condition at the transmitted front reads

$$\delta H_a(\theta_t, q_a) = \alpha_{a1}(q_a) \delta P_a(\theta_t, q_a) + \alpha_{a2}(q_a), \quad (59)$$

where

$$\alpha_{a1}(q_b) = \chi_a \sinh q_a + \frac{1}{2} \frac{\beta_t \kappa_t - \beta_t^2}{\kappa_t} \frac{\rho_{af}}{1 - \beta_t^2} \frac{1}{\rho_{a0} \sinh q_a}, \quad (60)$$

$$\alpha_{a2}(q_a) = -\delta v_{ya}^0 \frac{\sinh \theta_t}{\sinh q_a}, \quad (61)$$

where

$$\chi_a = \frac{\kappa_t + \beta_t^2}{2 \kappa_t \beta_t}.$$

Combining Eqs. (15), (16), (17), (53), (54), and (59), we arrive at the following system of four coupled functional equations:

$$\begin{aligned} \cosh(q_b + \theta_r) \eta_r^+(q_b + \theta_r) \delta P_r(q_b + \theta_r) + \alpha_{b2}(q_b + \theta_r) \\ = \delta H_{bi}(q_b) + \cosh q_b \delta P_{bi}(q_b), \end{aligned} \quad (62)$$

$$\begin{aligned} \cosh(q_b - \theta_r) \eta_r^-(q_b - \theta_r) \delta P_r(q_b - \theta_r) + \alpha_{a2}(q_b - \theta_r) \\ = \delta H_{bi}(q_b) - \cosh q_b \delta P_{bi}(q_b), \end{aligned} \quad (63)$$

$$\begin{aligned} \cosh(q_a + \theta_t) \eta_t^+(q_a + \theta_t) \delta P_t(q_a + \theta_t) + \alpha_{a2}(q_a + \theta_t) \\ = \delta H_{ai}(q_a) + \cosh q_a \delta P_{ai}(q_a), \end{aligned} \quad (64)$$

$$\begin{aligned} \cosh(q_a - \theta_t) \eta_t^-(q_a - \theta_t) \delta P_t(q_a - \theta_t) + \alpha_{a2}(q_a - \theta_t) \\ = \delta H_{ai}(q_a) - \cosh q_a \delta P_{ai}(q_a), \end{aligned} \quad (65)$$

where $\eta_r^\pm = [\alpha_{b1}(q_b)/\cosh q_b] \pm 1$ and $\eta_t^\pm = [\alpha_{a1}(q_a)/\cosh q_a] \pm 1$.

From the preceding equations it can be seen that $\delta P_r(q_b = 0) = -\lim_{q_b \rightarrow 0} [\alpha_{b2}/\alpha_{b1}]$ and similarly $\delta P_t(q_a = 0) = -\lim_{q_a \rightarrow 0} [\alpha_{a2}/\alpha_{a1}]$.

The task of solving Eqs. (62)–(65) is by far more complicated than that of solving the equivalent functional equation for only one shock, as we did in Eq. (35). The difficulty lies in the fact that θ_r and θ_t appear both adding and subtracting inside the unknown pressure functions. If we, for example, make the transformation $q_b \rightarrow q_b + \theta_r$ in Eq. (63), the variable q_a should be changed accordingly to the corresponding new value given by

$$\operatorname{arcsinh} \left(\frac{c_{af}}{c_{bf}} \sinh(q_b + \theta_r) \right),$$

which evidently complicates the desired iteration sequence. A similar difficulty arises if we make the transformation $q_a \rightarrow q_a - \theta_t$ in Eq. (64). The solution consists in rewriting the

former system in a more tractable form, reminiscent of Eq. (35). The best option that we have found is to express the Rankine-Hugoniot conditions at the shocks and the boundary conditions at the contact surface, in terms of the previously defined functions F_{m1} and F_{m2} .

In fact, going back to Eqs. (11), (12), and/or Eqs. (53) and (54), we can see that the pressure perturbations in fluid “ m ” can be written as

$$\delta P_m(\theta_m, q_m) = \frac{F_{m1}(q_m - \theta_m) + F_{m2}(q_b + \theta_m)}{\cosh q_m}, \quad (66)$$

$$\delta H_m(\theta_m, q_m) = F_{b1}(q_m - \theta_m) - F_{m2}(q_m + \theta_m). \quad (67)$$

The linearized Rankine-Hugoniot conditions at the shocks can be recast in the form

$$F_{a2}(q_a) = \frac{\delta v_{ya}^0 \sinh \theta_t - \sinh(q_a - \theta_t) \eta_t^-(q_a - \theta_t) F_{a1}(q_a - 2\theta_t)}{\sinh(q_a - \theta_t) \eta_t^+(q_a - \theta_t)}, \quad (68)$$

$$F_{b1}(q_b) = \frac{\delta v_{yb}^0 \sinh \theta_r - \sinh(q_b + \theta_r) \eta_r^+(q_b + \theta_r) F_{b2}(q_b + 2\theta_r)}{\sinh(q_b + \theta_r) \eta_r^-(q_b + \theta_r)}, \quad (69)$$

and the boundary conditions at the interface can be written as

$$F_{a2}(q_a) = \frac{2F_{b2}(q_b) - (\Delta - 1)F_{a1}(q_a)}{\Delta + 1}, \quad (70)$$

$$F_{b1}(q_b) = \frac{2\Delta F_{a1}(q_a) + (\Delta - 1)F_{b2}(q_b)}{\Delta + 1}, \quad (71)$$

where $\Delta = (\rho_{af} \cosh q_b) / (\rho_{bf} \cosh q_a)$.

After some straightforward algebra, Eqs. (68)–(71) can be reduced to the system

$$\phi_{a3} F_{a1}(q_a) + F_{b2}(q_b) = \phi_{a1} + \phi_{a2} F_{a1}(q_a - 2\theta_t), \quad (72)$$

$$F_{a1}(q_a) + \phi_{b3} F_{b2}(q_b) = \phi_{b1} + \phi_{b2} F_{b2}(q_b + 2\theta_r), \quad (73)$$

where the functions ϕ_{m1} , ϕ_{m2} , and ϕ_{m3} are straightforward combinations of the functions $\eta_{r,t}^\pm$ and Δ and are written in the Appendix. We can see that the preceding system of functional equations, despite still having coupled unknown functions, is easier to solve by the iterative procedure than the previous system of four equations. The new unknown functions are F_{a1} and F_{b2} . We need to relate the sonic interaction parameters F_a and F_b with these unknown functions. In order to get that relationship, we combine Eqs. (46), (47), (66), and (67) and use the results

$$\delta H_{bi}(q_b=0) = \delta H_{ai}(q_a=0) = -\delta v_i^\infty, \quad (74)$$

$$\begin{aligned} \rho_{bf} \delta P_{bi}(q_b=0) &= \rho_{bf} (\delta v_{yb}^\infty - \delta v_{yb}^0) = \rho_{af} (\delta v_{ya}^\infty - \delta v_{ya}^0) \\ &= \rho_{af} \delta P_{ai}(q_a=0). \end{aligned} \quad (75)$$

After some algebra, we arrive at the desired relationships:

$$F_a = \left[1 + \frac{4(u_t - v_i)}{v_i} \left(1 - \frac{\beta_r^2}{\kappa_r} \right)^{-1} \right]^{-1} [\delta v_{ya}^0 - 2F_{a1}(-2\theta_t)], \quad (76)$$

$$F_b = \left[1 + \frac{4(u_i + v_r)}{v_1 - v_i} \left(1 - \frac{\beta_r^2}{\kappa_r} \right)^{-1} \right]^{-1} [\delta v_{yb}^0 - 2F_{b2}(2\theta_r)]. \quad (77)$$

Thus, to get the growth rate, we have to solve for $F_{a1}(q_a = -2\theta_t)$ and $F_{b2}(q_b = 2\theta_r)$ and substitute them into Eqs. (76) and (77) and go to Eq. (3). We show how to solve the functional equations in the following subsection.

2. Solution of the functional equations

By looking at Eqs. (72) and (73), we realize that the system can be rewritten in matrix form. Actually, let us define

$$\mathbf{R} = \begin{pmatrix} -2(\Delta - 1)/(\Delta + 1)^2 & 4\Delta/(\Delta + 1)^2 \\ 4\Delta/(\Delta + 1)^2 & 2\Delta(\Delta - 1)/(\Delta + 1)^2 \end{pmatrix}, \quad (78)$$

$$\mathbf{T} = \mathbf{R} \cdot \begin{pmatrix} \phi_{a2} e^{-2\theta_t D_a} & 0 \\ 0 & \phi_{b2} e^{2\theta_r D_b} \end{pmatrix}. \quad (79)$$

Therefore, Eqs. (72) and (73) can be set in the form

$$\mathbf{F} = \mathbf{R}\Phi_0 + \mathbf{T}\mathbf{F}, \quad (80)$$

where $\mathbf{F} = (F_{a1}(q_a), F_{b2}(q_b))$, $\Phi_0 = (\phi_{a1}, \phi_{b1})$.

The matrix \mathbf{T} must be understood as an operator acting on the vector \mathbf{F} . Let us define $\Xi_0 = \mathbf{R}\Phi_0$. Then, Eq. (80) can be solved by iteration in the usual way:

$$\mathbf{F}^{[n]} = \Xi_0 + \mathbf{T}\mathbf{F}^{[n-1]}, \quad (81)$$

provided we have an initial function with which to start the iteration process. We try the same procedure as we did to solve the single shock problem in the preceding subsection. We consider the original functional equation system in the limit of very large q_m values, neglecting the shock coordinates inside the arguments of the unknown functions. In this way, we arrive at a simple linear algebraic system in the unknown functions. But we do not neglect the front coordinates inside the arguments of the ϕ functions, because this improves the convergence velocity of the iteration process. We get for the function F_{b2} ,

$$F_{b2}^{[0]}(q_b) = \frac{\phi_{a1} - \phi_{b1}(\phi_{a3} - \phi_{a2})}{1 - (\phi_{b3} - \phi_{b2})(\phi_{a3} - \phi_{a2})}. \quad (82)$$

As for the starting function to be used in place of $F_{a1}^{[0]}$, it is much better to go back to the *original* functional equations system and get $F_{a1}^{[0]}$ from Eq. (73):

$$F_{a1}^{[0]} = \phi_{b1} - \phi_{b3}F_{b2}^{[0]}(q_b) + \phi_{b2}F_{b2}^{[0]}(q_b + 2\theta_r). \quad (83)$$

There is an important reason for doing so. In the preceding equation, we are taking advantage of the fact that the function $F_{b2}^{[0]}$ is being evaluated at the corresponding value of q_b and also at $q_b + 2\theta_r$. If we realize that in general the reflected shock front is rather weak, even for very strong incident shocks, we can deduce that the shock front coordinate θ_r will be large. This means that we are evaluating $F_{b2}^{[0]}$ at large values of its argument. Taking into account that the $F_{m,2}$ functions behave as decaying exponentials, we can easily realize that the correcting terms added by the successive iterations will be smaller and smaller. That is, in reflecting through the contact surface into fluid ‘‘b’’ [by means of Eq. (73), as we did before], we are taking advantage of the fact that the shifts inside the trial functions are quite substantial in fluid ‘‘b.’’

Let us further define $\mathbf{F}^{[0]} = (\mathbf{F}_{a1}^{[0]}, \mathbf{F}_{b2}^{[0]})$. Then, a formal solution to the original system of functional equations can be written as

$$\begin{aligned} \mathbf{F} &= \lim_{n \rightarrow \infty} (\mathbf{\Xi}_0 + \mathbf{T}\mathbf{\Xi}_0 + \mathbf{T}^2\mathbf{\Xi}_0 + \mathbf{T}^3\mathbf{\Xi}_0 + \dots + \mathbf{T}^{(n-1)} \\ &\quad \times \mathbf{\Xi}_0 + \mathbf{T}^n\mathbf{F}^{[0]}). \end{aligned} \quad (84)$$

We have obtained the solution to the perturbation problem. Using either Eqs. (81) or (84), we can get the sonic parameters and finally calculate the growth rate. The very interesting property of the method just outlined is that the convergence speed is very high, and with a couple of iterations we can cover the relevant regions of the initial space of physical parameters already studied in the literature.

III. RESULTS

A. Comparison with previous simulations

Let us consider a shock coming from air and impinging upon a corrugated surface that separates it from SF₆. In Fig. 4, we show the growth rate (in units of $k\psi_0u_i$, as will be all the growth rates in this subsection) as a function of the incident shock intensity [defined as in Ref. [3]: $s = (p_1 - p_0)/p_1$]. The gases parameters are $\gamma_{\text{air}} = 1.4$, $\gamma_{\text{SF}_6} = 1.0935$, and $\rho_{\text{SF}_6}/\rho_{\text{air}} = 5.1$. We also plot the predictions of Eqs. (1) and (2). The triangles indicate the simulation results taken from Yang *et al.* [3]. We see very good agreement between the numerical results and the prediction of Eq. (3) even in the high compression limit. Unfortunately, the impulsive formulas separate from the exact result at relatively low Mach numbers (~ 1.5). In applying Eq. (3) to infer the results presented in Fig. 4, we have used in general the starting functions. Only in the strong shock limit ($s > 0.8$) have we begun to increase the value of the iteration index (n). For very strong shocks ($s \sim 1$), we have used $n = 3$ to get three significant digits. However, even using the starting func-

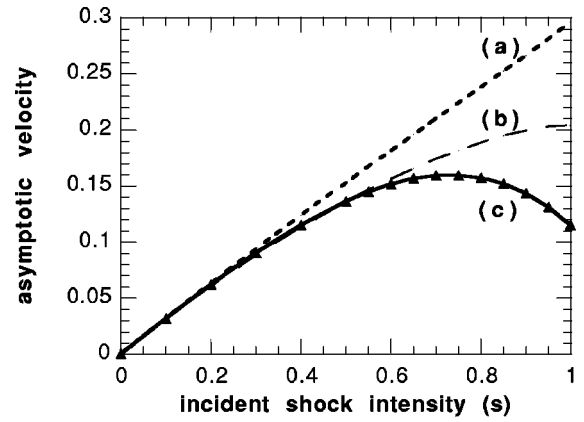


FIG. 4. Asymptotic growth rate δv_i^∞ as a function of the incident shock intensity for the gases air-SF₆. The fluid parameters are $\gamma_a = 1.0935$, $\gamma_b = 1.4$, $\mathcal{R}_0 = 5.1$. The curve (a) is the prediction of the VMG model [9]. The curve (b) corresponds to the impulsive model of Richtmyer [1] and the curve (c) is obtained with Eq. (3). The triangles are the simulation results of Yang *et al.* [3].

tion ($n = 0$), we get for the growth rate the value 0.129, which differs by less than 20% from the exact value (which is 0.115). The impulsive models give for this case a difference on the order of 100% (R prescription) or more (VMG model).

Next, in Table I, we also compare with the predictions of Yang *et al.* [3]. We have used only the starting functions for the majority of the cases indicated there, except those marked with one asterisk (which means that $n = 1$ was used in the iteration sequence) or with two asterisks ($n = 2$). Higher iteration steps were needed for very strong incident shocks and very compressible fluids at either side of the contact surface. An amazing result is the fact that we can reproduce the indirect phase inversion observed in case (c), with just the starting function, even though it corresponds to a very strong incident shock.

The fact that a negative growth rate can be detected for some combinations of the initial parameters is an indication of the possibility of freeze-out. Indeed, if we increase slightly the value of the initial density ratio at the interface, we find that the growth rate should change sign somewhere in the interval $1.13307 < \rho_{a0}/\rho_{b0} < 1.13308$. The accurate determination of the initial conditions that may result in the instability freeze-out could be very useful to the research community in ICF [5]. However, an exhaustive study of the parameter space searching for freeze-out conditions on the basis of Eq. (3) is something well beyond the scope of the present work and will be left for the future.

B. Comparison with recent experiments in shock tubes

Quite recently [21], a set of experiments in a shock tube for the case in which a shock reflects back in the lighter fluid has been performed. The light gas was N₂ and the heavier gas SF₆ (we consider the properties of N₂ to be the same as those of air as far as our model is concerned). Weak shock waves were generated with Mach ~ 1.10 . The novelty of these experiments was the absence of a plastic membrane in

TABLE I. Asymptotic growth rate as given by Eq. (3) and the numerical simulations of Yang *et al.* [3]. The left column is the incident shock intensity (defined in the text), the top row is the preshock density ratio. The upper number in each entry is the result given by Eq. (3) and the lower one is the result shown in Table I of Yang *et al.* [3]. The two adiabatic exponents are (a) $\gamma_a = \gamma_b = 1.1$, (b) $\gamma_a = \gamma_b = 3.0$, and (c) $\gamma_a = 3.0, \gamma_b = 1.5$.

s	ρ_{a0}/ρ_{b0}				
	1.1	2.0	4.0	8.0	16.0
1.0	0.004 02	0.0312*	0.0639**	0.0933**	0.114**
	0.0040	0.031	0.064	0.094	0.11
0.5	0.0151	0.0929	0.141	0.150	0.135
	0.015	0.093	0.14	0.15	0.13
0.05	0.002 07	0.0123	0.0179	0.0183	0.016
	0.0021	0.012	0.018	0.018	0.016
(a)					
1.0	0.0141	0.0893	0.141*	0.156*	0.144*
	0.014	0.089	0.14	0.16	0.14
0.5	0.008 18	0.0492	0.0723	0.0746	0.0657
	0.0081	0.049	0.072	0.075	0.065
0.05	0.0078	0.004 64	0.006 74	0.006 85	0.005 96
	0.0078	0.0046	0.0067	0.0068	0.0060
(b)					
1.0	-0.003 83	0.0711	0.143	0.187*	0.197*
	-0.0038	0.071	0.14	0.19	0.20
0.5	0.004 02	0.006 43	0.101	0.107	0.0958
	0.0040	0.0064	0.10	0.11	0.095
0.05	0.001 20	0.007 36	0.0104	0.0104	0.0089
	0.0012	0.0073	0.010	0.010	0.0089
(c)					

order to separate the gases before the shock traversed the interface. They produced a nearly flat interface by causing the two gases to collide and by providing slots for the fluids to escape through the tube walls. For details of the experimental conditions, we refer the reader to the original work [21].

As the experiments involved only weak shocks, the role of the sonic parameters is not very important in this case. Only the initial circulation deposited by the fronts at the interface at $t=0+$ is enough to get an estimate of the asymptotic growth rate. Anyway, it is worthwhile to attempt a comparison between their results and the prediction of our Eq. (3).

They have presented their measurements for the growth rate as the slope of the corrugation amplitude versus (zero-

order) interface displacement. That is, their value corresponds to the quantity $d\Psi_i/dX_i$, where Ψ_i is the corrugation amplitude at the contact surface and X_i is actually $v_i t$ in our notation. For their experimental conditions—Mach ≈ 1.10 and $k\psi_0 \approx 0.13$ —they obtained $(d\Psi_i/dX_i)_{\text{expt}} \approx 0.0875 \pm 0.0078$.

Our irrotational prediction [the first term in Eq. (3)] is $(d\Psi_i/dX_i)_{\text{irrot}} \approx 0.0834$. This value is in quite good agreement with their experimental result. If we calculate the sonic interaction parameters for both gases and use the complete Eq. (3), we obtain $(d\Psi_i/dX_i)_{\text{Eq. (3)}} \approx 0.0824$, a value that cannot be distinguished from the experimental one within the measurement uncertainty. There is a small difference between the irrotational approximation and the complete Eq. (3) (less than 5%). This difference, impossible to discern with experimental measurement, is mainly due to the SF_6 , which is very compressible. Before closing the discussion, we must note that our results are only exact for a sharp interface. The authors of the experiment have taken into account that the experimental interface could be diffuse rather than strictly sharp. Unfortunately, a self-consistent theory of the Richtmyer-Meshkov instability for diffuse interfaces does not yet exist to our knowledge. Nevertheless, we can follow the same strategy as used by Jones and Jacobs and modify Eq. (3) with the growth reduction factor (GRF) used in that work [21]. The authors modified the Richtmyer impulsive formula for a diffuse interface by solving an eigenvalue equation. For the conditions of their experiments, they have obtained $\text{GRF} \approx 1.17$. Using this value, we get $(d\Psi_i/dX_i)_{\text{irrot}} \approx 0.0713$ within the irrotational approximation and $(d\Psi_i/dX_i)_{\text{Eq. (3)}} \approx 0.0705$ including the sonic parameters in both gases. We see that considering the growth reduction factor, we underestimate the observed asymptotic growth rate by an amount that goes beyond the experimental uncertainty. Summing up, the theoretical predictions of our model seem to be in good agreement with these experiments considering a sharp interface instead of a diffuse one. We also see, in agreement with our expectations, that the role played by the vorticity deposited ahead of the contact surface, in the bulk of the SF_6 and N_2 gases, is not very important due to the low intensity of the incident shock.

IV. FINAL DISCUSSION

Before closing the work, it is important to make some brief remarks on the high speed of convergence seen in the calculations. As mentioned before, there are two main reasons. One is the fact that we are taking advantage of the relative “weakness” of the reflected shock. This causes the reflected shock parameter θ_r to be in general larger than 1. Besides, the sound speed of the fluid “b” is in general larger than the sound speed in fluid “a.” Any time we reflect the interesting quantities (like the function F_{a1}) to the other side of the contact surface through Eq. (73), we gain a large shift in the iteration process. This shift, being substantial on side “b,” accelerates considerably the overall convergence, because the correcting terms added at each successive step will be smaller, due to the monotonicity property of the trial functions at large values of their arguments. Physically, we are

exploiting the fact that in the space between the reflected shock and the contact surface, there are fewer sound-wave reverberations than on the other side. The reason is always the same. The reflected front travels at almost the shocked speed of sound of fluid “*b*.” Therefore, any pressure perturbation emanating from the interface will barely arrive at the shock, because they go at almost the same speed [11]. This phenomenon does not happen on side “*a*,” except for very weak shocks. Then, the advantage of reflecting the unknown function F_{a1} into the fluid with higher sound velocity is evident.

However, as we have already discussed when studying the single perturbed shock, the most powerful reason is the special choice we have made of the starting function.

In fact, it is not difficult to arrive, within the framework of the model, at the following relationship for the reflected shock front pressure perturbations [see Eqs. (23), (66), and (69)]:

$$(\delta P_r^{[0]})_{q_b=0} = (\delta P_r)_{q_b=0} - \lim_{q_b \rightarrow 0} \frac{2F_{b2}^{[0]}(q_b + \theta_r)}{\eta_r^-(q_b)}. \quad (85)$$

It is easy to see that the functions η_r^\pm diverge in the limit $q_b \rightarrow 0$. Then, unless we choose for $F_{b2}^{[0]}$ a divergent function at $q_b = \theta_r$, regardless of the starting function we use, the corresponding initial guess for the shock front pressure perturbations will always start from the correct value at $q_b = 0$. This last fact is very useful, because it provides us with a great range of starting functions from which to choose. We just use the one that behaves correctly in the opposite limit: $q_b \gg \theta_r$. Physically, we are starting the calculations with a trial function that behaves correctly at early and large times. The subsequent iteration process fills the gap between both ends in order to satisfy the boundary conditions at both shocks and at the interface. The immediate advantage of the technique used is the reduction in the number of terms that must be retained to get a specified accuracy. To get three significant digits, the traditional series expansions could require hundreds of terms [16] and starting the calculations with high-precision arithmetic. In our case, we need at most a couple of iterations and we have no need of a huge number of digits to avoid round-off errors [4,11,16].

To summarize, we have presented an analytical model that correctly calculates the asymptotic growth rate of the Richtmyer-Meshkov instability for the case of a reflected shock. It takes into account the vorticity deposited initially by the deformed fronts at the contact surface and also succeeds in describing the later sonic interaction between the fronts and the interface. This interaction is important in the strong shock limit, that is, in the limit of high compressions. The model can be extended to deal with different situations that go beyond the classical Richtmyer-Meshkov problem: time-varying externally imposed pressure perturbations at the left boundary, etc. The model can be used in the search of the initial preshock conditions that could result in the freeze-out of the velocity perturbations. Good agreement with previous numerical and experimental work has been shown.

ACKNOWLEDGMENTS

This work has received partial support from PB970571 and FTN2000-2048-C03-02 of Ministerio de Educacion y Ciencia, Spain.

APPENDIX: AUXILIARY FUNCTIONS $\phi_{m,1,2,3}$

$$\phi_{a1} = \frac{\Delta + 1}{2} \frac{\delta v_{ya}^0 \sinh \theta_t}{\sinh(q_a - \theta_t) \eta_t^+(q_a - \theta_t)},$$

$$\phi_{a2} = -\frac{\Delta + 1}{2} \frac{\eta_t^-(q_a - \theta_t)}{\eta_t^+(q_a - \theta_t)},$$

$$\phi_{a3} = \frac{1 - \Delta}{2},$$

$$\phi_{b1} = \frac{\Delta + 1}{2\Delta} \frac{\delta v_{yb}^0 \sinh \theta_r}{\sinh(q_b + \theta_r) \eta_t^-(q_b + \theta_r)},$$

$$\phi_{b2} = -\frac{\Delta + 1}{2\Delta} \frac{\eta_r^+(q_b + \theta_r)}{\eta_r^-(q_b + \theta_r)},$$

$$\phi_{b3} = \frac{\Delta - 1}{2\Delta}.$$

-
- [1] R. D. Richtmyer, *Commun. Pure Appl. Math.* **13**, 297 (1960).
 [2] E. E. Meshkov, *Fluid Dyn.* **4**, 101 (1969).
 [3] Y. Yang, Q. Zhang, and D. H. Sharp, *Phys. Fluids* **6**, 1856 (1994).
 [4] A. L. Velikovich, *Phys. Fluids* **8**, 1666 (1996).
 [5] A. L. Velikovich, J. P. Dahlburg, A. J. Schmitt, J. H. Gardner, L. P. Phillips, F. L. Cochran, Y. K. Chong, G. Dimonte, and N. Metzler, *Phys. Plasmas* **7**, 1662 (2000).
 [6] J. G. Wouchuk and K. Nishihara, *Phys. Plasmas* **4**, 1028 (1997).
 [7] N. J. Zabusky, *Annu. Rev. Fluid Mech.* **31**, 495 (1999).
 [8] M. Brouillette and B. Sturtevant, *Physica D* **37**, 248 (1989).
 [9] M. Vandenboomgaerde, C. Mügler, and S. Gauthier, *Phys. Rev. E* **58**, 1874 (1998).
 [10] B. Dimonte, C. E. Frerking, M. Schneider, and B. Remington, *Phys. Plasmas* **3**, 614 (1996).
 [11] G. Fraley, *Phys. Fluids* **29**, 376 (1986).
 [12] J. G. Wouchuk and K. Nishihara, *Phys. Plasmas* **3**, 3761 (1996).
 [13] K. Mikaelian, *Phys. Fluids* **6**, 356 (1994).
 [14] K. O. Mikaelian, *Phys. Rev. Lett.* **71**, 2903 (1993).
 [15] M. G. Briscoe and A. A. Kovitz, *J. Fluid Mech.* **31**, 529 (1968).
 [16] A. L. Velikovich, J. P. Dahlburg, J. H. Gardner, and R. J.

- Taylor, Phys. Plasmas **5**, 1491 (1998).
- [17] T. L. Saaty, *Modern Non Linear Equations* (Dover, New York, 1981), p. 164.
- [18] C. Cohen-Tannoudji, B. Diu, and F. Laloë, *Quantum Mechanics* (John Wiley & Sons, New York, 1977), Vol. I, p. 190.
- [19] V. N. Goncharov, Phys. Rev. Lett. **82**, 2091 (1999).
- [20] R. Ishizaki and K. Nishihara, Phys. Rev. Lett. **78**, 1920 (1997); Phys. Rev. E **58**, 3744 (1998).
- [21] M. A. Jones and J. W. Jacobs, Phys. Fluids **9**, 3078 (1997).